

Molecular diversity of cell-matrix adhesions

Eli Zamir¹, Ben-Zion Katz², Shin-ichi Aota³, Kenneth M. Yamada², Benjamin Geiger¹ and Zvi Kam¹

¹Department of Molecular Cell Biology, The Weizmann Institute of Science, Rehovot, Israel

²Craniofacial Developmental Biology and Regeneration Branch, NIDCR, NIH, Bethesda, MD, USA

³Biomolecular Engineering Research Institute, Osaka, Japan

*Author for correspondence (e-mail: ligeiger@wicmail.weizmann.ac.il)

Accepted 25 March; published on WWW 11 May 1999

SUMMARY

In this study we have examined for molecular heterogeneity of cell-matrix adhesions and the involvement of actomyosin contractility in the selective recruitment of different plaque proteins. For this purpose, we have developed a novel microscopic approach for molecular morphometry, based on automatic identification of matrix adhesions, followed by quantitative immunofluorescence and morphometric analysis. Particularly informative was fluorescence ratio imaging, comparing the local labeling intensities of different plaque molecules, including vinculin, paxillin, tensin and phosphotyrosine-containing proteins. Ratio imaging revealed considerable molecular heterogeneity between and within adhesion sites. Most striking were the differences between focal contacts, which are vinculin- and paxillin-rich and contain high levels of phosphotyrosine, and fibrillar adhesions, which are tensin-rich and contain little or no phosphotyrosine. Ratio imaging also revealed considerable variability in the molecular substructure of individual focal contacts, pointing to a non-uniform

distribution of phosphotyrosine and the different plaque constituents. Studying the quantitative relationships between the various components of the submembrane plaque indicated that the levels of vinculin, paxillin and phosphotyrosine in adhesion sites are positively correlated with each other and negatively correlated with the levels of tensin. Tyrosine phosphorylation of focal contacts was highly sensitive to cellular contractility, and was diminished within 5 minutes after treatment with the kinase inhibitor H-7, an inhibitor of actomyosin contractility. This was followed by the loss of paxillin and vinculin from the focal adhesions. Tensin-rich fibrillar adhesions were relatively insensitive to H-7 treatment. These findings suggest a role for contractility in the generation of matrix adhesion diversity.

Key words: Focal contact, Cell adhesion, Ratio imaging, Computerized microscopy

INTRODUCTION

Focal contacts (FC) are specialized adhesion sites formed between cultured cells and the underlying extracellular matrix (ECM) (Burrige and Fath, 1989; Geiger et al., 1995; Gilmore and Burrige, 1996; Yamada and Geiger, 1997). In these regions, originally identified by electron microscopy (Abercrombie et al., 1971; Heath and Dunn, 1978) or by interference reflection microscopy (Abercrombie and Dunn, 1975; Izzard and Lochner, 1976), cells form close and tight adhesions to the underlying substratum. At their cytoplasmic aspects, FC are associated with bundles of actin filaments through an electron-dense, multi-molecular complex, the submembrane plaque. In typical adherent cultured cells a large number (tens to hundreds) of distinct FC can be detected, ranging in size from less than a square micron to several square microns. The number of FC, their size and distribution, can vary greatly from one cell to the other or even within a single cell, and their morphological diversity may be affected by multiple factors including the nature of the substratum, composition of the culture medium, incubation time after plating, and cell density.

During the last several years, considerable information has accumulated on the molecular composition of FC. It was shown that the transmembrane 'adhesion receptors' present in these sites are members of the integrin superfamily (Hynes, 1987, 1992; Schwartz et al., 1995). These molecules react, through their ecto-domains, with specific ECM molecules, and through their cytoplasmic tails with components of a submembrane plaque that links them to the microfilament system (Geiger et al., 1995; Yamada and Geiger, 1997). This plaque contains a multitude of proteins, some of which participate in the physical linkage of the membrane receptors to the cytoskeleton, while others are signal transduction molecules, including different protein kinases, their substrates and various adapter proteins (Geiger et al., 1995; Jockusch et al., 1995; Kam et al., 1995; Yamada and Geiger, 1997). It is believed that the recruitment of these molecules to FC and their activation plays a central role in the generation of 'adhesion signals' that are involved in the regulation of many cellular processes such as cell growth, differentiation or apoptosis (Clark and Brugge, 1995; Schwartz et al., 1995; Yamada, 1997; Yamada and Geiger, 1997). Recent studies have indicated that the assembly of FC is also stimulated by local tyrosine-specific

protein phosphorylation and that the phosphorylation events are triggered by tension applied to the FC-anchored adhesion complexes by the attached bundles of actin filaments (Bershadsky et al., 1996).

It is intriguing that despite the extensive work for over two decades and the vast information available on FC formation and organization, a definitive and unequivocal molecular characterization of these structures is not yet available. For example, it is not clear whether all submembrane plaques are basically equivalent at a molecular level, nor how their composition is regulated. An application of computerized morphometry was reported recently to analyze gravitational effects on vinculin and FC morphology (Usson et al., 1997), but little is known about the molecular classes, organization and quantitative dynamics of these adhesion sites.

To approach these questions, we have developed a microscopic system that enables us to perform detailed quantitative morphometry of matrix adhesions. In this report we describe this experimental approach and its application to evaluate two hypotheses: (a) cell-matrix adhesions may not be uniform, but may instead consist of a range of distinct structures that differ at the molecular level between and within individual adhesions; and (b) it may be possible to switch on or off rapidly the phosphorylation and assembly state of mature cell-matrix adhesions within minutes.

For rigorous, quantitative testing of these and other concepts in cell-matrix adhesion, we present here a detailed procedure for automated identification of matrix adhesions and characterization of their properties including their size, axial ratio and labeling intensity for their various constituents, as well as the calculation of fluorescence ratio imaging (FRI). This digital microscopy approach was applied here to cultured fibroblasts to test for the extent and types of molecular heterogeneity of their matrix adhesions. The results revealed an unexpected level of variability in the composition of these matrix adhesions, extending even to different regions within the same adhesion site. Our findings establish three general categories of adhesion sites within a broad spectrum of populations of matrix adhesions, namely 'classical FC' which are extensively labeled for paxillin, vinculin and phosphotyrosine, 'fibrillar adhesions' which contain relatively low levels of these characteristic proteins and instead contain high levels of tensin, and 'mosaic adhesions' which contain a combination. We also show that treatment with the kinase inhibitor H-7, which blocks actomyosin contraction (Volberg et al., 1994; Tian et al., 1998) leads to a rapid loss of phosphotyrosine from FC, which is then followed by their dissociation. We further show that very shortly (<5 minutes) after H-7 withdrawal, well-formed FC with apparently normal morphology and composition suddenly reconstitute, indicating a high degree of potential plasticity.

MATERIALS AND METHODS

Cell culture and immunofluorescence staining

Rat embryo fibroblasts (REF52) were plated on glass coverslips in Dulbecco's modified Eagle's medium (DMEM) supplemented with 10% fetal calf serum. For immunofluorescence labeling cells were fixed-permeabilized with 3% paraformaldehyde, 0.5% Triton X-100 in PBS for 2 minutes, and post-fixed with 3% paraformaldehyde in

PBS for 30 minutes. The cells were then washed with PBS and stained with the primary antibodies for 1 hour. After washing with PBS, the cells were stained with the secondary antibodies, namely Cy3- or FITC-conjugated goat anti-mouse or goat anti-rabbit IgG. Finally, the cells were washed with PBS and mounted in Elvanol (Mowiol 4-88, Hoechst, Frankfurt, Germany).

H-7-induced inhibition of contractility

To inhibit cellular contractility, REF52 cells were incubated with 60 μ M 1-(5-iso-quinoliny)sulfonyl)-2-methylpiperazine (H-7; I-7016, Sigma Chemical Co., St Louis, MO, USA) for different periods of time (Volberg et al., 1994; Tian et al., 1998). The cells were then fixed and double-labeled as described. Recovery was achieved by removal of the H-7-containing medium and further incubation of the cells in normal growth medium.

Immunochemical reagents

The primary antibodies used in this study included: rabbit anti-vinculin (R695, Geiger 1979), rabbit anti-phosphotyrosine (PT40, kindly provided by Israel Pecht and Arie Licht, The Weizmann Institute), monoclonal antibody (mAb) anti-vinculin (clone hVin-1, Sigma Chemical Co., St Louis, MO, USA), and mAbs anti-paxillin and anti-tensin (Transduction Laboratories, Lexington, KY, USA). Secondary antibodies (all from Jackson ImmunoResearch Laboratories Inc., West Grove, PA, USA) were Cy3-conjugated goat anti-rabbit F(ab')₂ fragment, Cy3-conjugated goat anti-mouse IgG H+L, FITC-conjugated F(ab')₂ fragment goat anti-mouse antibody and FITC-conjugated goat anti-rabbit IgG F(ab')₂ fragment.

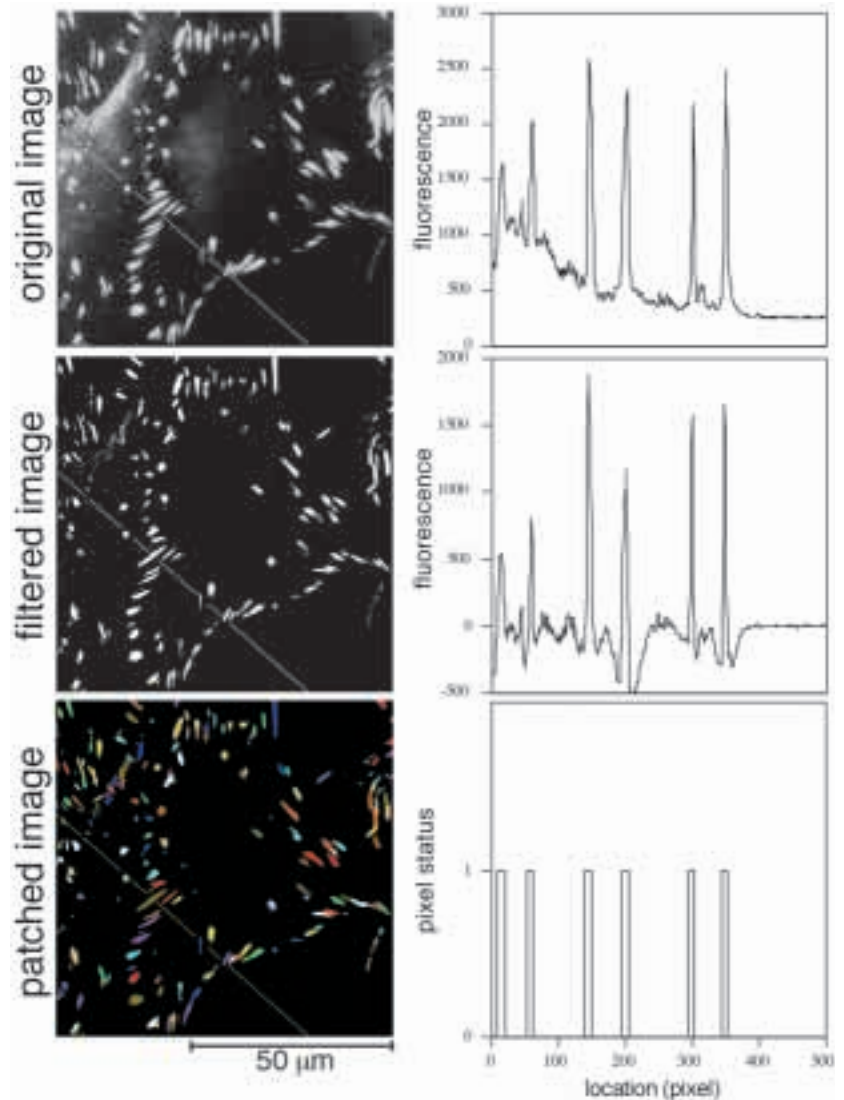
Generation of GFP-cytoskeletal molecules chimeric proteins

Full-length chicken vinculin cDNA (Bendory et al., 1989; Price et al., 1989) and full-length human paxillin cDNA (kindly provided by K. Nakata, S. Miyamoto and K. Matsumoto, National Institute of Dental and Craniofacial Research, National Institutes of Health, Bethesda, MD) were ligated in-frame into pGZ21 vector according to the method of Kioka et al. (1999). pGZ21 contains a cytomegalovirus promoter and a green fluorescent protein (GFP) coding sequence with three amino acid residue substitutions (S65A, V68L, and S72A) to increase its fluorescence in mammalian cells (Cormack et al., 1996). REF52 cells were transfected using the calcium phosphate method (Sambrook et al., 1989). Expression of each fusion protein was verified at the protein level by western blotting utilizing monoclonal antibodies to vinculin or paxillin, as well as anti-GFP monoclonal antibody (data not shown). As an additional control, full-length chicken tensin was also expressed as a GFP fusion protein (B.-Z. Katz, K. Matsumoto, S. Aota, D. Lin, S. Lin and K. M. Yamada, unpublished).

Computerized immunofluorescence microscopy

Specimens were examined using an Axioskop microscope (Zeiss, Oberkochen, Germany) with selective fluorescence excitation and emission interference filters and quad-dichroic mirror (Chroma, VT, USA) that were positioned in the optical path by computer-driven filter wheels. Images were acquired using a scientific-grade cooled charged-coupled device (CCD) camera (Model C220, Photometrics Co., AZ, USA) with Texas Instruments 1024 \times 1024 pixels chip readout generating 12-bit digital data. Image acquisition and processing were controlled by a Silicon Graphics workstation model 4D/35 (Mountain View, CA, USA) using modified Resolve3D and Prism software (Chen et al., 1990, 1995; Kam et al., 1993, 1997). This system is currently produced by Applied Precision Inc. (Issaquah, WA, USA). In the present study cells were examined with a \times 100/1.3NA plan-Neofluar objective (Zeiss, Oberkochen, Germany) resulting in a pixel length of 0.118 μ m. In order to correct for non-homogenous illumination and pixel-to-pixel variations in CCD sensitivities, correction files were prepared from a slide containing a thin layer of homogenous solution of rhodamine, using the Resolve3D software,

Fig. 1. Main stages in the segmentation of adhesion sites. Left, top: a typical fluorescence image of vinculin-labeled REF52 cells. Note the relatively high diffuse fluorescence in the perinuclear area, which is common to many immunolabeled preparations. Left, middle: the same field after high-pass filtration (box size: 40×40 pixels). The diffuse background fluorescence disappeared while FC patches, including relatively small and faint ones, remained unchanged. Left, bottom: segmented ‘patches’, corresponding to vinculin-labeled matrix adhesions, as calculated by the *water* software. To distinguish individual adhesions, they are artificially marked by random colors, demonstrating the separation of adjacent adhesions. Right column: for each image, a one-dimensional plot of fluorescence intensity along the marked broken line is presented. The upper and middle panels present the fluorescence intensity along this line in the original and filtered image, respectively. The 6 narrow peaks in each graph correspond to 6 FC crossed by the line. The broad labeling that existed in the original image, but not in the high-pass filtered image, corresponds to the diffuse staining in the perinuclear region. The bottom panel indicates the status of each pixel along this line in the patched image, where each pixel is either included in (‘status’ = 1) or excluded from (‘status’ = 0) a segmented patch.



and applied during the acquisition session. To ensure accurate alignment between the Cy3 image and the FITC image, cells were immunofluorescently stained for vinculin using a monoclonal anti-vinculin antibody followed by a mixture of Cy3-conjugated and FITC-conjugated goat anti-mouse antibodies. This slide was then used to measure, and correct, small shifts between the Cy3 and the FITC images. These shifts were found to remain constant during the acquisition session (Kam et al., 1995).

Image filtration

Matrix adhesions, immunolabeled for their constituent proteins, appear as local intensity maxima (‘patches’) at the substrate focal plane. However, images often contain diffuse background, which is especially prominent in thick regions of the cell. Subtraction of the averaged image intensity within a rectangular box around each pixel (Eq. 1, Fig. 1), for a box size larger than matrix adhesions, but small compared to cell dimensions, ‘flattens’ this background (‘high-pass filtered image’, P_{ij}^f) and facilitates interactive determination of a uniform threshold level, P_{\min}^f , that is well below staining intensity for all matrix adhesion patches, yet is above noise. The box-filter was chosen since it can be implemented in a fast algorithm. The box size used in this study was 4.7×4.7 μm. Following segmentation (see below); intensities and background levels were calculated from the unfiltered P_{ij} images.

Equation 1

High-pass filtration

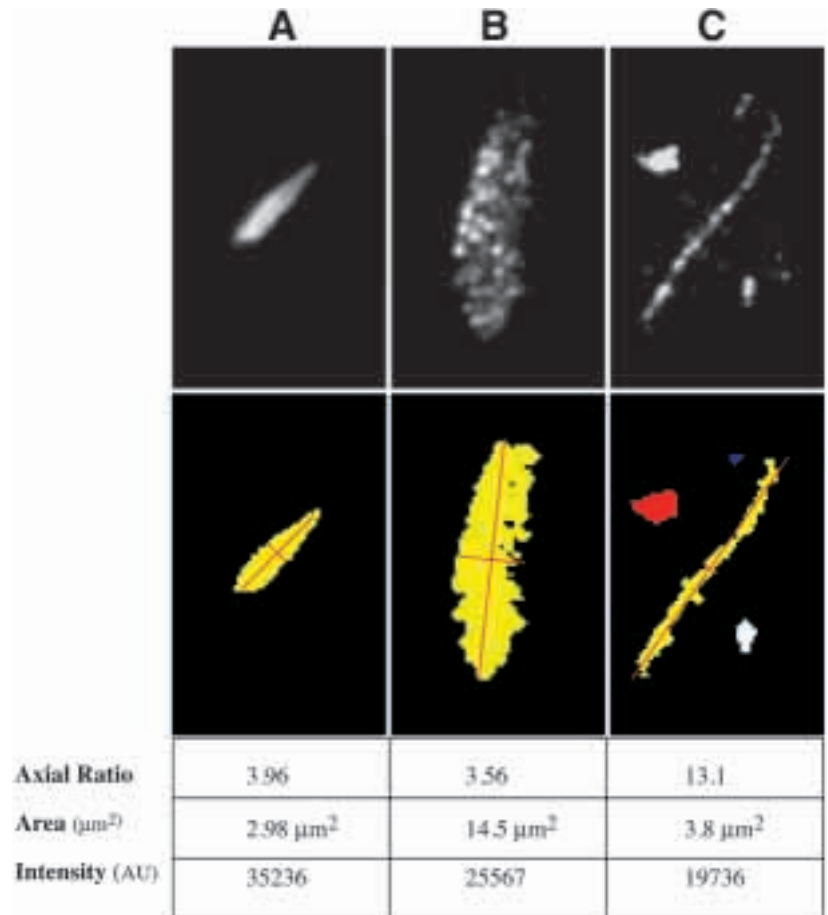
$$P_{ij}^f = P_{ij} - \frac{\sum_{q=i-b}^{i+b} \sum_{w=j-b}^{j+b} P_{qw}}{(2b+1)^2},$$

where P_{ij} and P_{ij}^f are the intensities of pixel ij in the original and the filtered image, respectively. $(2b+1)^2$ defines a constant rectangular area, equivalent to 4.7×4.7 μm.

Segmentation and quantitation of matrix adhesions

Image segments corresponding to individual matrix adhesions (‘patches’) were defined using a segmentation algorithm we named ‘*water*’, which is based on a modified ‘lake’ algorithm (Soferman, 1989). Usually, all adhesion sites in 4 representative cells were used as a basis for generation of quantitative data sets for each treatment. The *water* algorithm can be visually described as the emergence of peaks and their associated slopes as water recedes from a hilly landscape after a flood. As water declines, new peaks appear (local maxima) and existing hills expand their area. When two previously disjointed mountains meet, the decision to merge them, or to regard them as separate identities, depends on their size. The algorithm is implemented

Fig. 2. Morphometry of matrix adhesions. Three morphologically distinct types of adhesions recognized by the *water* software are shown: (i) an arrowhead-shaped structure with homogenous fluorescence intensity (A); (ii) a large structure with a granular texture (B); (iii) a thin and elongated ‘beaded’ structure (C). The upper row presents the original images, and the lower row presents the segmented image as defined by the *water* software. The short (R_k^{short}) and long (R_k^{long}) axes of the ellipses best fitted to these structures are indicated by red lines. The calculated axial ratios (L_k , Eq. 4), areas (A_k , Eq. 2) and average intensities (I_k , Eq. 5) of each structure are indicated.



for 2-D and 3-D images for any desired pixel connectivity, but was applied here in 2-D with 4-neighbors connectivity (i.e. each pixel has 4 touching neighbors: up, down, right and left; all the other diagonal pixels are not considered connected). The inputs for the *water* routine are: the filtered image (P_{ij}^f), a threshold for minimum pixel intensity (P_{min}^f), a threshold for minimum patch area (A_{min}^p) and a critical patch size for merging (A_{min}^m). The output assigns a patch number M_{ij} to each pixel (ij), or zero to pixels that do not belong to any patch. The set of instructions in the *water* routine can be described as follows:

1. Sort the (ij) pixels in the high-pass filtered image according to their intensity (P_{ij}^f), forming a list in a decreasing order.

2. Cycle over pixels (ij) in the sorted order, until $P_{ij}^f < P_{min}^f$. At each cycle, the pixel (ij) either:

Case 1. Forms a new patch, if it is not touching any existing patch.

Case 2. Is assigned to an existing patch, if it is touching one.

Case 3. Merges patches, if it is touching more than one, and the size of at least one of the connected patches is below the critical area for merging (A_{min}^m) (otherwise it is assigned to the first patch it touches).

3. Exclude all patches smaller than the minimum area for patches A_{min}^p .

The critical area for merging was typically set at 40 pixels ($0.56 \mu\text{m}^2$). This value was empirically found to prevent fragmentation of matrix adhesions due to their internal structure, yet allowed separation of adjacent, yet distinct, matrix adhesions. To identify very large matrix adhesions with a granular texture, the critical area for merging was set to a much higher value of 300 pixels ($4.2 \mu\text{m}^2$).

The *water*-generated mask, M_{ij} (Fig. 1) allows calculation for each matrix adhesion ('patch') of various morphometric and fluorescent attributes based on the original image data (Fig. 2). The morphometric parameters used in this study include: area (Eq. 2), center of mass (Eq. 3), axial ratio of best-fitted ellipse (Eq. 4), intensity (Eq. 5), and the

ratio between the intensities of two fluorophores (i.e. Cy3 and FITC) for each patch (for double-labeled samples). The equations used for calculating these parameters are listed below:

Equation 2

Patch area, A_k :

$$A_k = \sum_{\{ij|M_{ij}=k\}} 1.$$

Equation 3

Patch center of mass (i_k^c, j_k^c)

$$i_k^c = \frac{\sum_{\{ij|M_{ij}=k\}} P_{ij} * i}{T_k}; j_k^c = \frac{\sum_{\{ij|M_{ij}=k\}} P_{ij} * j}{T_k},$$

where the total intensity within patch k is:

$$T_k = \sum_{\{ij|M_{ij}=k\}} P_{ij}.$$

Equation 4

Patch axial ratio, L_k :

$$L_k = \frac{R_k^{long}}{R_k^{short}},$$

where R_k^{long} and R_k^{short} are the length of the long and the short axes of

the ellipse best fitted to patch k . This ellipse axes were obtained by calculating the Eigen values of the second moment matrix for $P_{ij}(ij|M_{ij}=k)$.

Equation 5

Patch intensity, I_k :

$$I_k = \frac{T_k}{A_k} - B_k .$$

The background intensity, B_k , is averaged locally from pixels around the patch k that do not belong to any other patch.

$$B_k = \frac{\sum_{\{ij|M_{ij}=0 \text{ and } (i-i_k^c)^2+(j-j_k^c)^2 < R^{long*1.2}\}} P_{ij}}{\sum_{\{ij|M_{ij}=0 \text{ and } (i-i_k^c)^2+(j-j_k^c)^2 < R^{long*1.2}\}} 1} .$$

Fluorescence ratio imaging (FRI)

Images of cells, double-labeled by immunostaining for two protein components of matrix adhesions, were acquired, high-pass filtered and aligned as described above. The high-pass filtration is critical for FRI since it abolishes the contribution of the background to the matrix adhesion intensity, and since it enables separation of background noise from the signal by a single threshold level. The ratio image was then computed and displayed (as schematically shown in Fig. 3). In order to avoid large ratio values due to low-intensity pixels in the denominator, the ratio is clipped below some set threshold. Nevertheless, it is important to include in the ratio image information about the presence of labeling in the numerator, even when the denominator is below threshold. For this purpose the ratio image was calculated with two separate thresholds for the numerator and denominator images, and assigned to each pixel in the ratio image values according to the following considerations: (A) If both

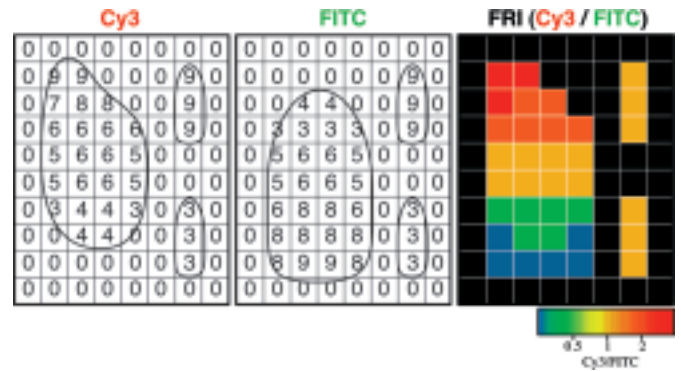


Fig. 3. Fluorescence ratio imaging (FRI). A schematic presentation of ratio imaging. The values within each square indicate the light intensity of the corresponding pixels in the Cy3 and FITC images, following high-pass filtration and thresholding. A value of zero is assigned to pixels with intensity lower than the threshold P_{min}^i for both fluorophores. The ratio image, calculated as described, is presented in the right panel. Note that: (a) pixels that are Cy3 positive and FITC-negative are marked red and those that are Cy3-negative and FITC-positive are marked blue, and (b) ratio values (and colors) are not sensitive to the absolute intensity (compare, for example, the two patches on the right).

numerator and denominator images were below threshold the ratio image was set to zero. (B) If numerator was below threshold, but denominator was above threshold, the ratio image was set to 0.1. (C) If the numerator was above threshold, but the denominator was below threshold the ratio image was set to 10. (D) When both images had pixel values above their respective thresholds, the ratio value was displayed in spectral, log scale, color look-up table (blue at minimum

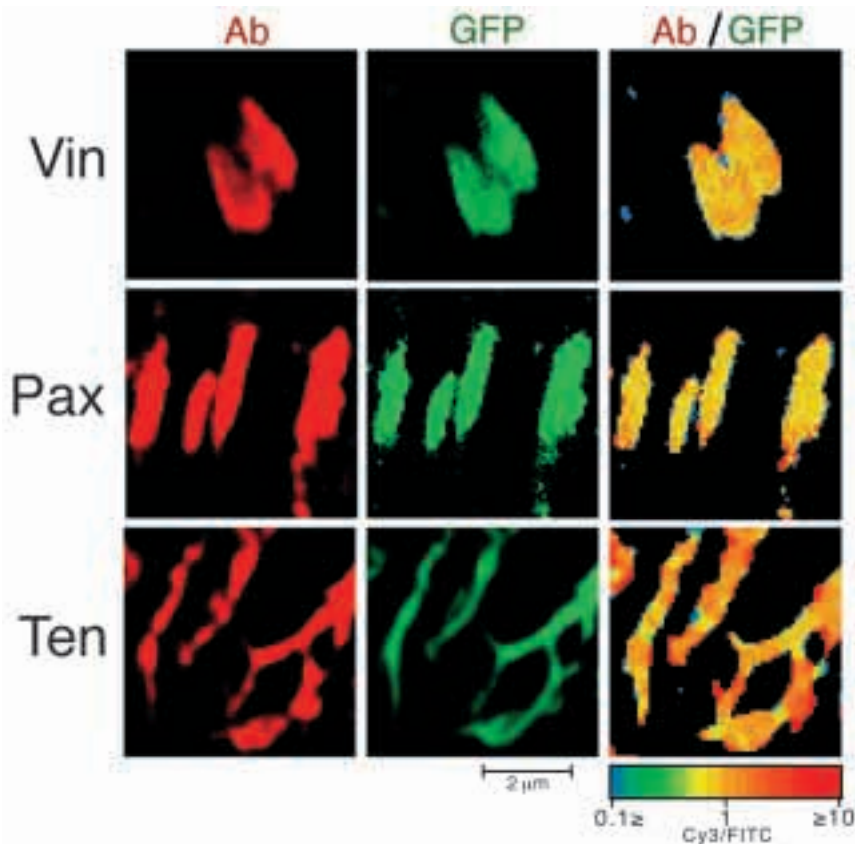


Fig. 4. Immunostaining and FRI of GFP-tagged FC proteins. REF52 cells, transfected with GFP-vinculin (Vin), GFP-paxillin (Pax) or GFP-tensin (Ten) chimeras, were fixed and immunostained with primary antibodies against the respective proteins (vinculin, paxillin or tensin), followed by Cy3-conjugated secondary antibodies. The rows present the Cy3 images in red, the GFP images in green and the fluorescence ratio images in a spectrum scale representing the ratio value.

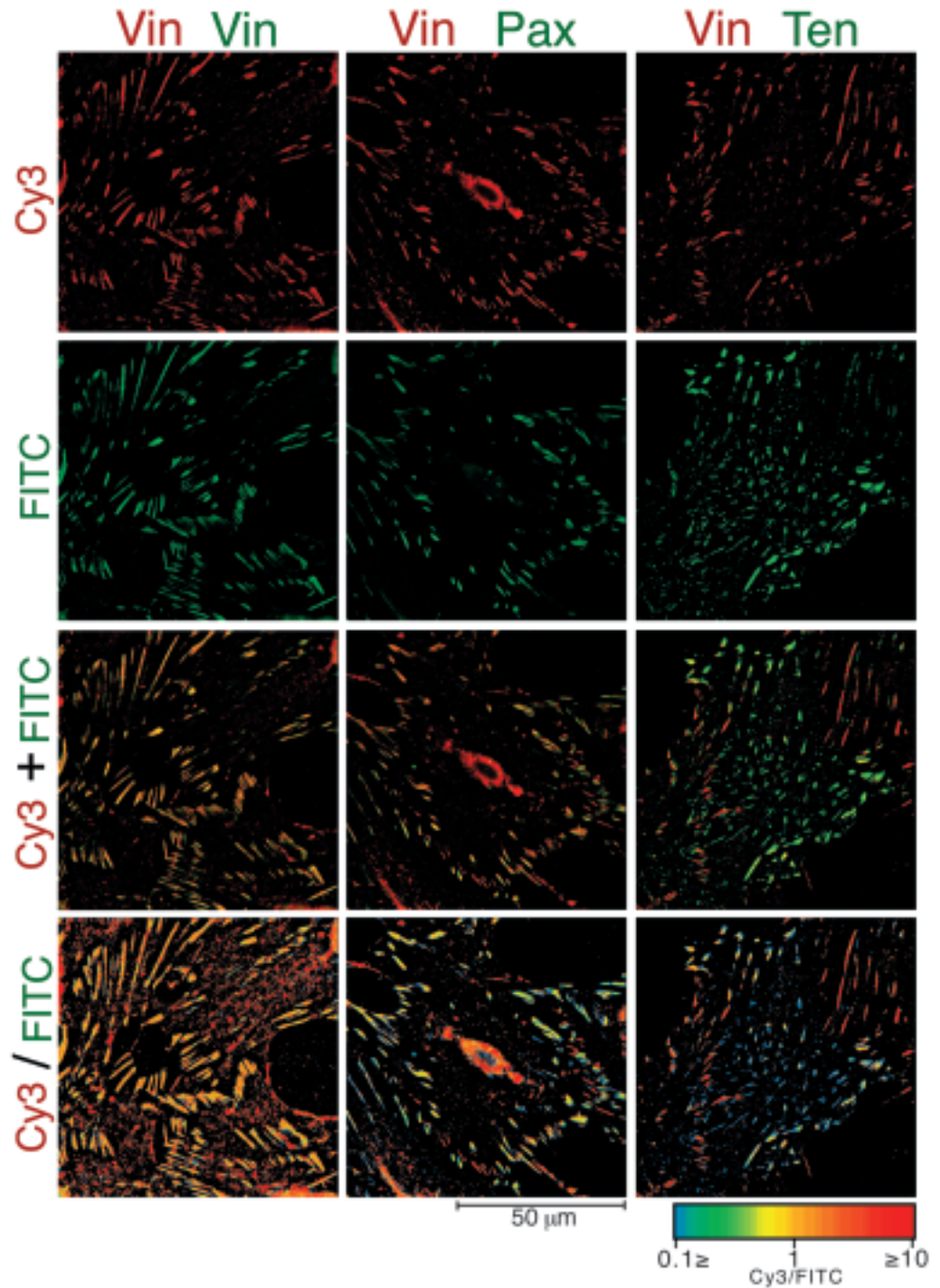


Fig. 5. FRI of vinculin and either paxillin or tensin. REF52 cells, 48 hours after plating, were double-labeled for vinculin and paxillin or vinculin and tensin using Cy3- and FITC-labeled antibodies, as indicated. The left column presents two-color labeling for vinculin, which was used as a control. The protein names are colored red for Cy3 and green for FITC labeling (Vin, vinculin; Pax, paxillin; Ten, tensin). The rows present, from top to bottom, the Cy3 images in red, the FITC images in green, the superimposed images in red and green, and the ratio images in a spectrum scale representing the value of the ratio. Note the uniform yellow color of FC in the control vinculin/vinculin ratio image due to uniform ratios of superimposed red and green.

to red at maximum), which permitted presentation of ratio value variations over two orders of magnitude (from 0.1 to 10). To utilize this range optimally, and to compensate for the differences in binding constants and photon yields of different secondary antibodies, all the ratios were normalized linearly by a constant that shifts their average toward a ratio of 1. The ratio image was then scaled from 0.1 to 10, assigning a black color to case A, blue to case B, red to case C, and a color corresponding to the spectral scale that corresponds to the ratio between the Cy3 intensity and the FITC intensity to case D.

FRI of GFP-tagged versus immunofluorescently-labeled FC was performed by transfecting REF52 cells with cDNA encoding GFP-fusion proteins of vinculin, paxillin or tensin. Forty-eight hours later

the cells were fixed and immuno-labeled with antibodies to vinculin, paxillin or tensin (respectively), and Cy3-conjugated secondary antibodies. FRI between the GFP and the Cy3 images was performed as described above.

RESULTS

Automated recognition and segmentation of cell-substrate adhesion sites

FC of REF52 cells were labeled for vinculin and automatically

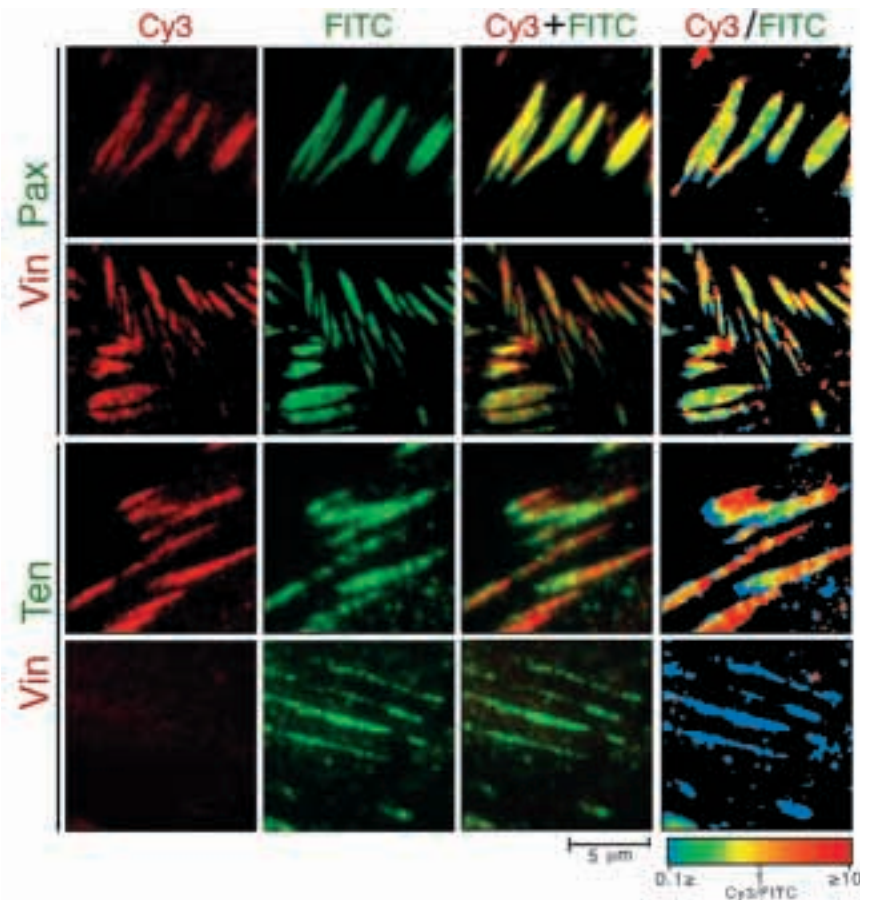


Fig. 6. Variations in the distribution of vinculin, paxillin and tensin within individual matrix adhesions. Double labeling and FRI images of individual adhesion sites following double labeling of REF52 cells for vinculin and either paxillin or tensin. Cells were labeled, and images are presented, as described in the legend for Fig. 5. The individual adhesions are shown here at a higher magnification, to visualize their internal molecular sub-structure.

identified as described above (Fig. 1). The raw images of such cells were often quite noisy, displaying diffuse staining in the nucleus or in a relatively thick region of the cytoplasm (Fig. 1, 'original image'). This background labeling was reduced using the high-pass filter, generating a relatively high-contrast image without losing small or faint FC (Fig. 1, 'filtered image'). Using the *water* algorithm, individual matrix-adhesion sites could be identified and marked either by a dot on the original raw image (not shown) or by random color presentation (Fig. 1, 'patched image'). The *water* system was capable of distinguishing close or even touching, yet distinct, adhesion sites. Rarely, apparently single adhesions were subdivided by the *water* algorithm into two or more smaller FC due to the presence of fine substructures within the FC itself. Such FC could be merged manually. For each matrix-adhesion site, the area, axial ratio, and intensity of patches recognized by the *water* software were calculated (Fig. 2). In order to segment very large and granular adhesion sites (Fig. 2B,C) we used a different set of threshold values for *water* segmentation from those used to recognize the more homogeneous and smaller FC.

Molecular diversity of cell-matrix adhesions – FRI analysis

To determine whether the immunofluorescence labeling intensity indeed represents the local concentrations of the various proteins, we transfected cells with cDNA encoding GFP chimeras of vinculin, paxillin or tensin, and 48 hours later (after the GFP-tagged molecules were fully incorporated into

adhesion sites) the cells were fixed and counter-labeled with antibodies to vinculin, paxillin or tensin, and then Cy3-labeled secondary antibodies. FRI of such double labeling experiments (Fig. 4) indicated that, for the three proteins tested, FRI values were highly uniform, confirming that the immunofluorescence labeling intensity accurately represents the local concentration of the respective proteins.

To study the level of molecular heterogeneity of matrix adhesions, REF52 were fixed 48 hours after plating, and double-labeled for different pairs of plaque proteins, using a mouse/rabbit combination of primary antibodies and the corresponding FITC- and Cy3-labeled secondary antibodies. The pairs of primary antibodies used here included: vinculin-paxillin, tensin-vinculin, phosphotyrosine-paxillin, tensin-phosphotyrosine, and phosphotyrosine-vinculin. All of these components were previously known to localize to FC (Geiger et al., 1995; Yamada and Geiger, 1997). As a control for the reliability of the double-labeling approach, we calculated the vinculin-vinculin FRI following double labeling with rabbit and mouse antibodies.

Examination of this control sample (vinculin-vinculin, Fig. 5, left column) revealed uniform ratio values both between and within FC. These nearly identical values of fluorescence ratios were found irrespective of local variations in vinculin labeling intensity. Minor differences apparently do not correspond to definitive FC, and reflect low levels of diffuse background labeling. Vinculin-paxillin FRI (Fig. 5, middle column) revealed largely comparable distributions of the two proteins in FC. Some sites, displaying vinculin-rich structures

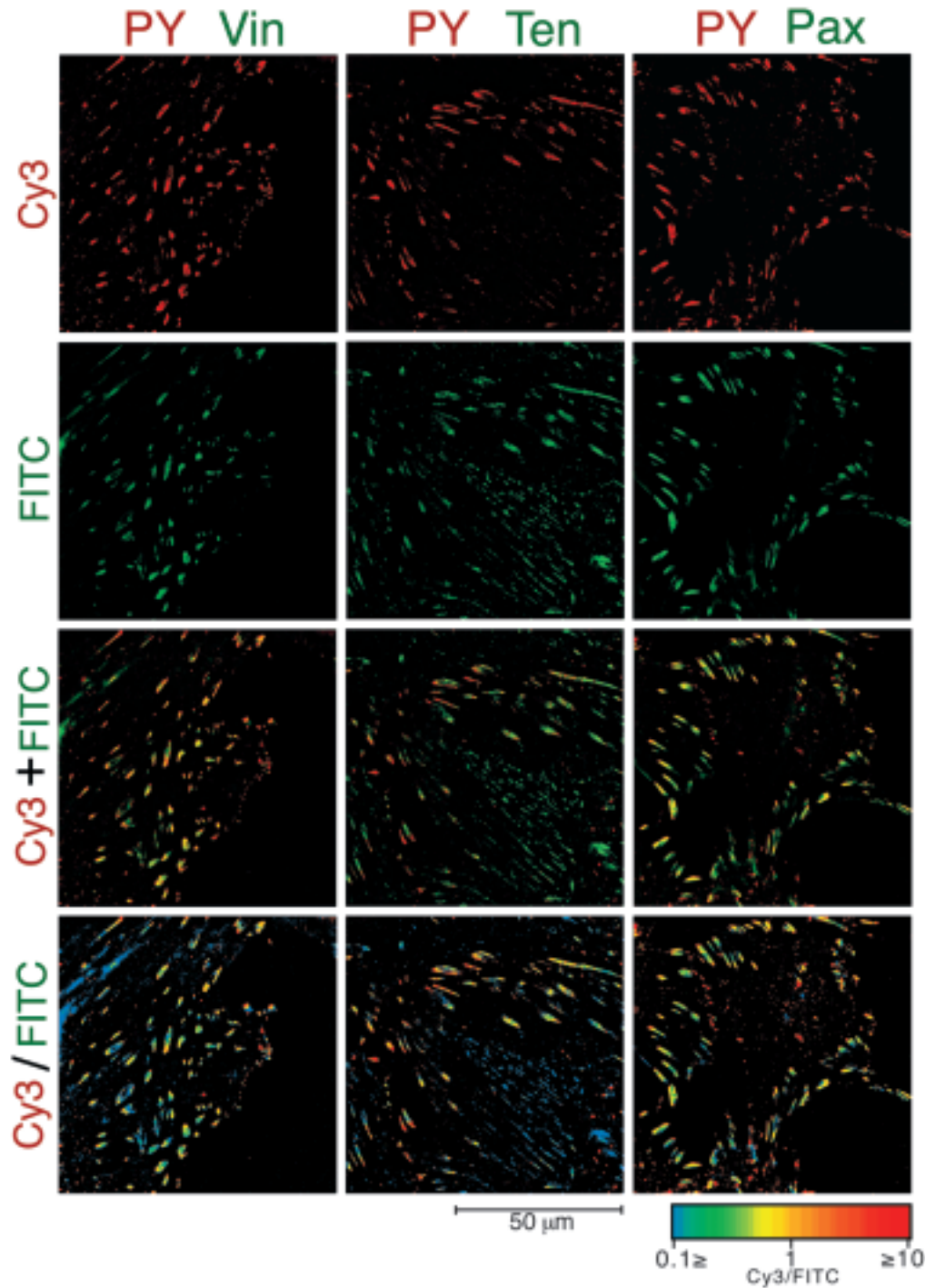


Fig. 7. FRI of phosphotyrosine and either vinculin, paxillin or tensin. REF52 cells, 48 hours after plating, were double-labeled for phosphotyrosine (PY) and either vinculin, tensin or paxillin, using Cy3- and FITC-labeled antibodies as indicated. The protein names are colored red for Cy3 and green for FITC labeling (Vin, vinculin; Pax, paxillin; Ten, tensin). The rows present, from top to bottom, the Cy3 images in red, the FITC images in green, the superimposed images in red and green, and the ratio images in a spectrum scale representing the value of the ratio.

with essentially no paxillin, corresponded to cell-cell adhesions, which were previously shown to contain vinculin but no paxillin (Turner et al., 1990). Examination of the tensin-vinculin pairs revealed very different distribution patterns (Fig. 5, right column). Three distinct types of adhesions were discerned: centrally-located adhesions which were tensin-rich, elongated FC at the cell periphery that were vinculin-rich, and smaller FC that displayed comparable fluorescence intensities of both proteins. These three populations were not randomly interspersed, but rather clustered in different regions of the cell (Fig. 5). Examination

at higher power revealed highly non-uniform distributions of the two proteins, with distinct tensin-rich or vinculin-rich domains within individual adhesions (Fig. 6). High magnification images of vinculin-paxillin FRI (Fig. 6) were largely uniform both within and between FC.

In view of the involvement of tyrosine phosphorylation in FC assembly (Ayalon and Geiger, 1997; Clark and Brugge, 1995; Gilmore and Burridge, 1996; Miyamoto et al., 1995; Volberg et al., 1992; Yamada and Geiger, 1997; Yamada and Miyamoto, 1995), we have compared the distribution of phosphotyrosine to that of paxillin, tensin or vinculin. Phosphotyrosine-paxillin

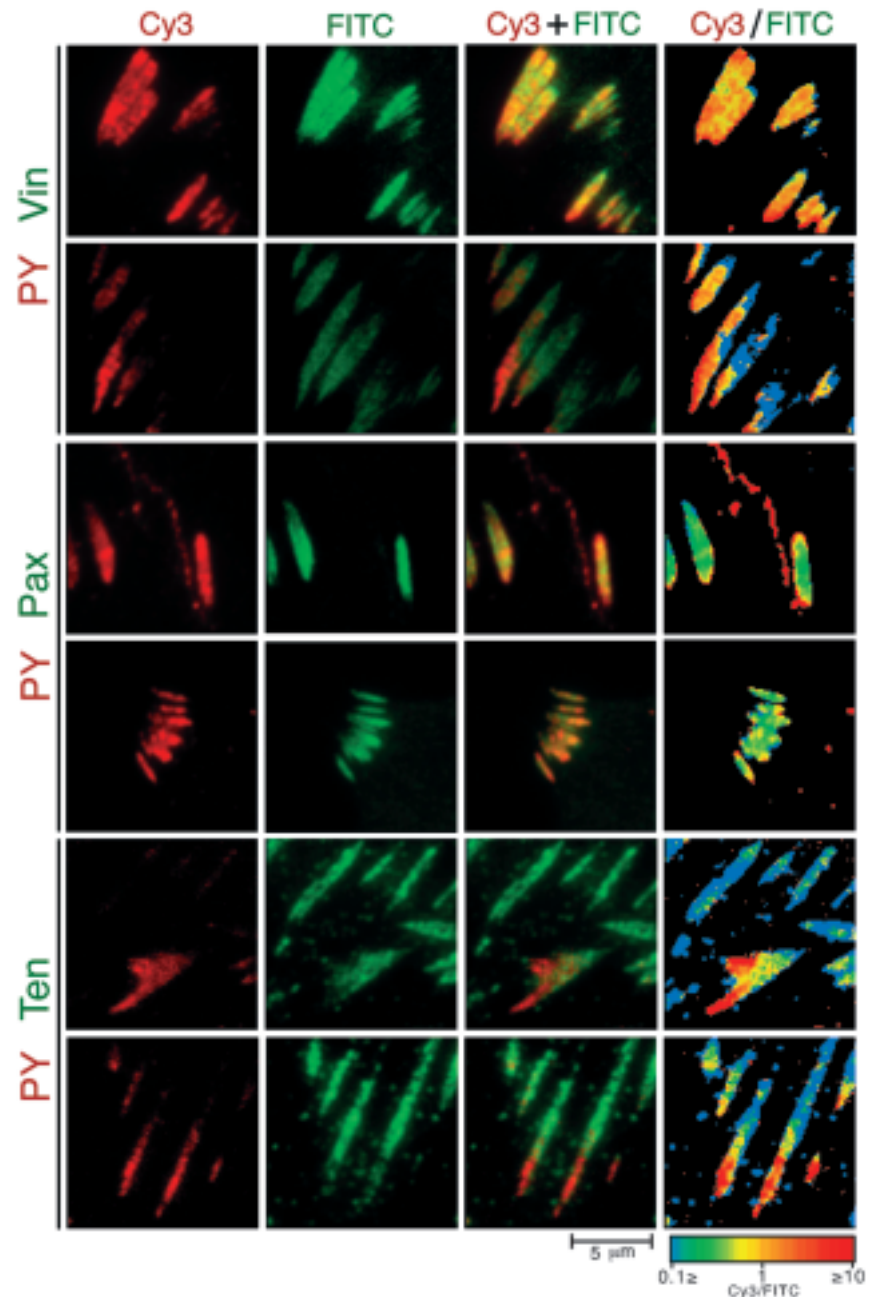


Fig. 8. Variations in the distribution of phosphotyrosine, vinculin, paxillin and tensin within individual matrix adhesions. Double labeling and FRI images of individual matrix adhesions following double labeling of REF52 cells for phosphotyrosine and either vinculin, paxillin or tensin (as in Fig. 6). Images are presented as described in the legend to Fig. 5.

FRI pointed to a largely similar labeling of FC with uniform FRI (Fig. 7). Again, occasional phosphotyrosine-labeled paxillin-negative structures at the cell periphery corresponded to cell-cell adherens junctions. Vinculin-phosphotyrosine FRI showed less uniform patterns both between and within FC (Fig. 7). The most striking differences observed, however, were between phosphotyrosine and tensin (Fig. 7) manifested by low ratios along the tensin-rich fibrillar adhesions located mainly at the cell center, and 'mosaic' FRI images in more peripheral FC pointing to mutually exclusive distribution. Examination of individual adhesions revealed that in contrast to vinculin and paxillin, phosphotyrosine was non-uniformly distributed along FC and tended to be associated with the edges or the periphery of FC (Fig. 8). Phosphotyrosine levels in fibrillar adhesions were very low compared to tensin (Fig. 8). Moreover, even

when tensin and phosphotyrosine were associated with the same structure, they usually did not overlap (Fig. 8).

To study the relationships between the morphology and composition of matrix adhesions, cells were labeled for tensin and phosphotyrosine, and the labeling intensities were correlated with the morphology of the adhesion sites. Phosphotyrosine was found to be primarily localized in round-to-ellipsoid (axial ratio <7) adhesions measuring $0.5\text{--}4\ \mu\text{m}^2$ (Fig. 9A,B,C). In contrast, tensin was associated with three distinct types of structures: (i) small ($0.5\text{--}3\ \mu\text{m}^2$) and rounded-to-ellipsoid (axial ratio <5) adhesions, (ii) elongated fibrillar structures (axial ratio >7), and (iii) large ($>8\ \mu\text{m}^2$) and rounded-to-ellipsoid (axial ratio <7) adhesions (Fig. 9A,B,C). In the non-fibrillar structures, the intensities of tensin and phosphotyrosine were variable compared to the rather uniform

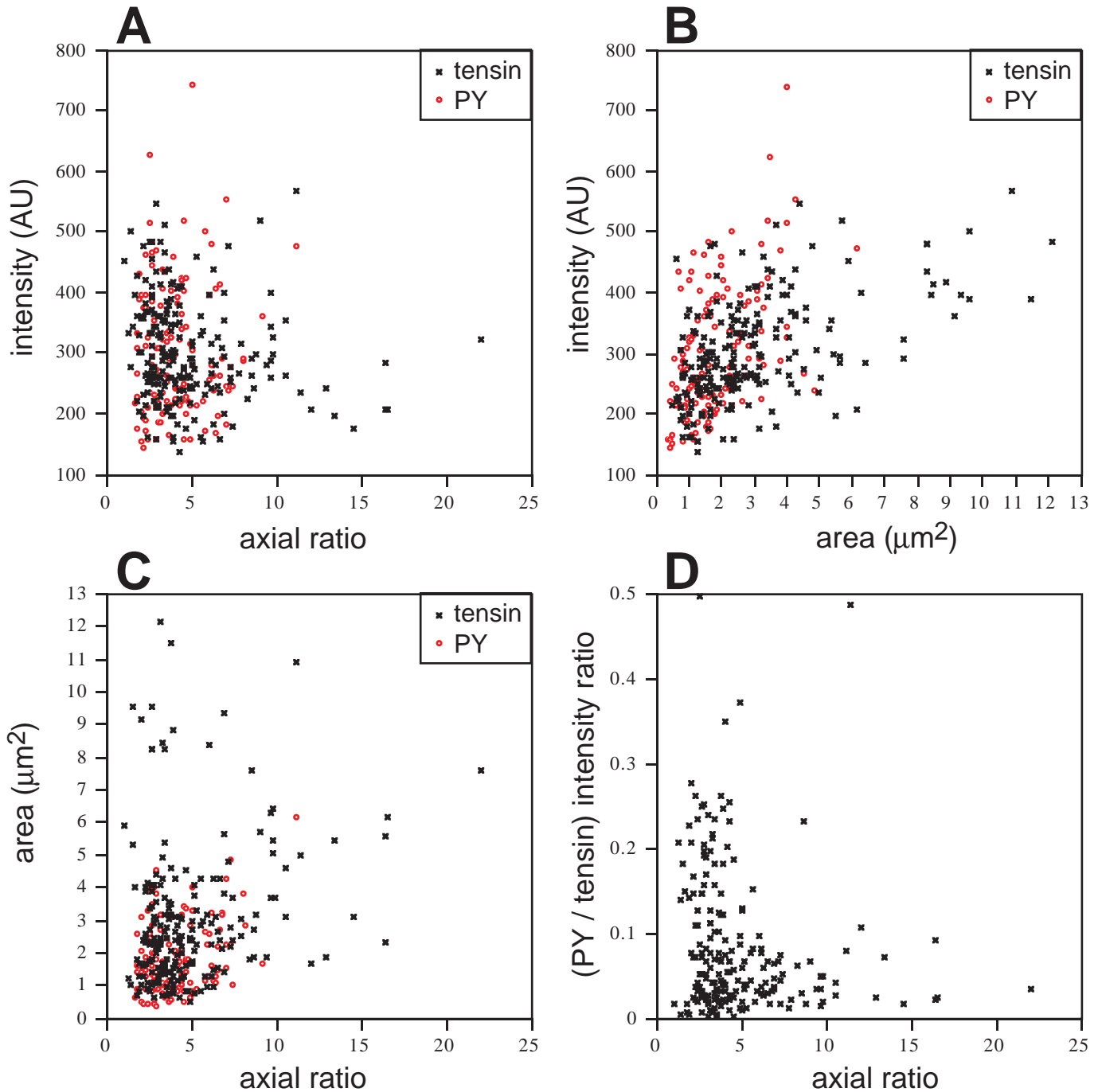


Fig. 9. Correlation between composition and morphological parameters in matrix adhesion sites. REF52 were double-stained for phosphotyrosine and tensin. The adhesion sites in four representative cells were segmented according to each type of staining separately, using the *water* algorithm. (A), (B) and (C) are scatter plots presenting the relationships between axial ratio (L_k , Eq. 4), intensity (I_k , Eq. 5) and area (A_k , Eq. 2) of adhesion sites segmented according to tensin labeling (black 'x') or phosphotyrosine labeling (red 'o'). (D), Scatter plot presenting the relationship between axial ratio and the phosphotyrosine to tensin fluorescence ratio. Segmentation was based on tensin labeling.

prevalence of tensin in, and the absence of phosphotyrosine from, the fibrillar structures (Fig. 9A, compare to D). These results established the existence of different molecular forms of adhesion sites with distinct shapes.

Quantitative evaluation of matrix adhesion diversity

To quantitatively determine the molecular relationships

between different constituents of cell-matrix adhesions, we compared the labeling intensities of vinculin and phosphotyrosine in matrix adhesions to those of vinculin (control), paxillin and tensin (Fig. 10). As expected, the relation between the paired labeling for vinculin was linear, positive, and with a high coefficient of correlation ($R=0.83\pm 0.04$). Paxillin labeling was also found to be strongly

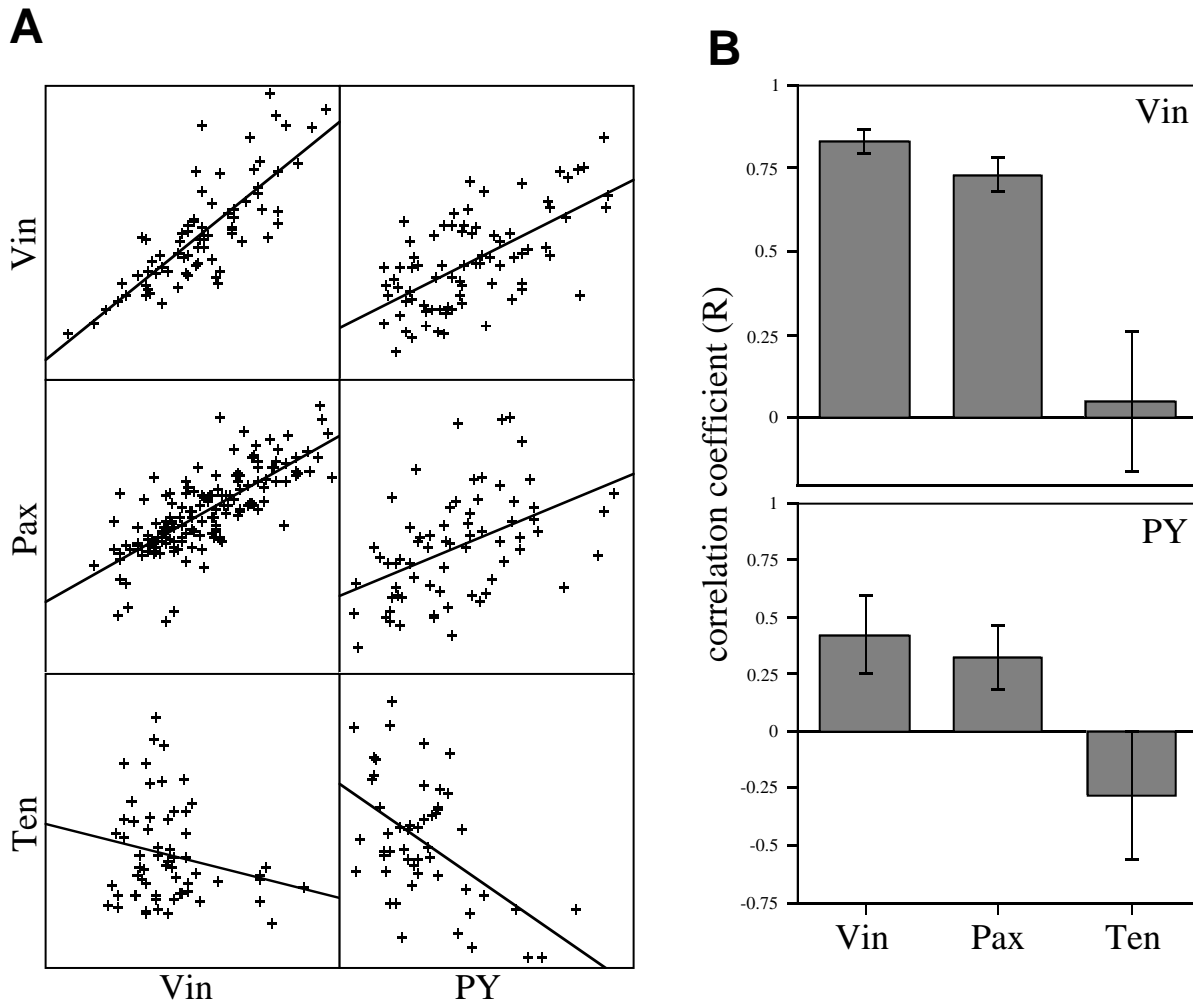


Fig. 10. Correlation between the labeling intensities of adhesion sites for different component molecules. REF52 were double-stained for vinculin or phosphotyrosine (with rabbit antibodies) and for vinculin or paxillin or tensin (with mouse mAb). Adhesion sites, in several representative cells per each paired staining, were segmented by the *water* software according to the vinculin or phosphotyrosine staining, and the intensities in the segmented areas were calculated for each of the proteins. (A) Scatter plots and regression lines presenting the relationships between the intensities (I_k , Eq. 5) of the double-stained proteins, in a representative cell (per each staining). (B) The calculated average values of the coefficient of correlation between the labeling intensities for the two respective proteins.

correlated with that of vinculin ($R=0.73\pm 0.08$; Fig. 10). Tensin, on the other hand, showed no significant correlation with vinculin ($R=0.05\pm 0.21$; Fig. 10).

Correlation of phosphotyrosine labeling intensity and that of paxillin, vinculin and tensin provided further insight into the molecular diversity of matrix adhesions. Both vinculin and paxillin were found to be positively correlated with phosphotyrosine intensities ($R=0.42\pm 0.17$ and $R=0.32\pm 0.14$, respectively), though the correlation coefficients were significantly lower than those obtained for the paxillin-vinculin pair. Tensin on the other hand was negatively correlated with the phosphotyrosine average intensity ($R=-0.28\pm 0.28$; Fig. 10).

Effect of cellular contractility on the molecular organization of matrix adhesions

As previously shown, treatment of cells with the kinase inhibitor H-7 leads to the loss of cellular contractility and deterioration of stress fibers and FC (Volberg et al., 1994; Tian et al., 1998). To monitor the dynamics of the molecular

changes occurring in adhesion sites due to the modulation of actomyosin contractility, we treated REF52 cells with $60\ \mu\text{M}$ H-7 and examined the morphology and molecular organization of adhesion sites.

As shown in Fig. 11, after 5 minutes of treatment with H-7, FC still had normal morphology and contained vinculin, paxillin and tensin, yet their phosphotyrosine content was dramatically reduced. Upon longer treatment FC gradually disappeared, and within 30 minutes almost no FC with normal morphology were retained; only dot-like structures containing paxillin and phosphotyrosine could be detected at the cell periphery. Tensin, in these H-7-treated cells, was primarily found in small, scattered patches that were largely devoid of phosphotyrosine, paxillin and vinculin. The nature of these structures is still unclear. A similar effect was also noted following treatment of human foreskin fibroblasts with a specific myosin light chain kinase inhibitor, ML-7 (data not shown).

This effect of H-7 was rapidly reversible, and well-formed

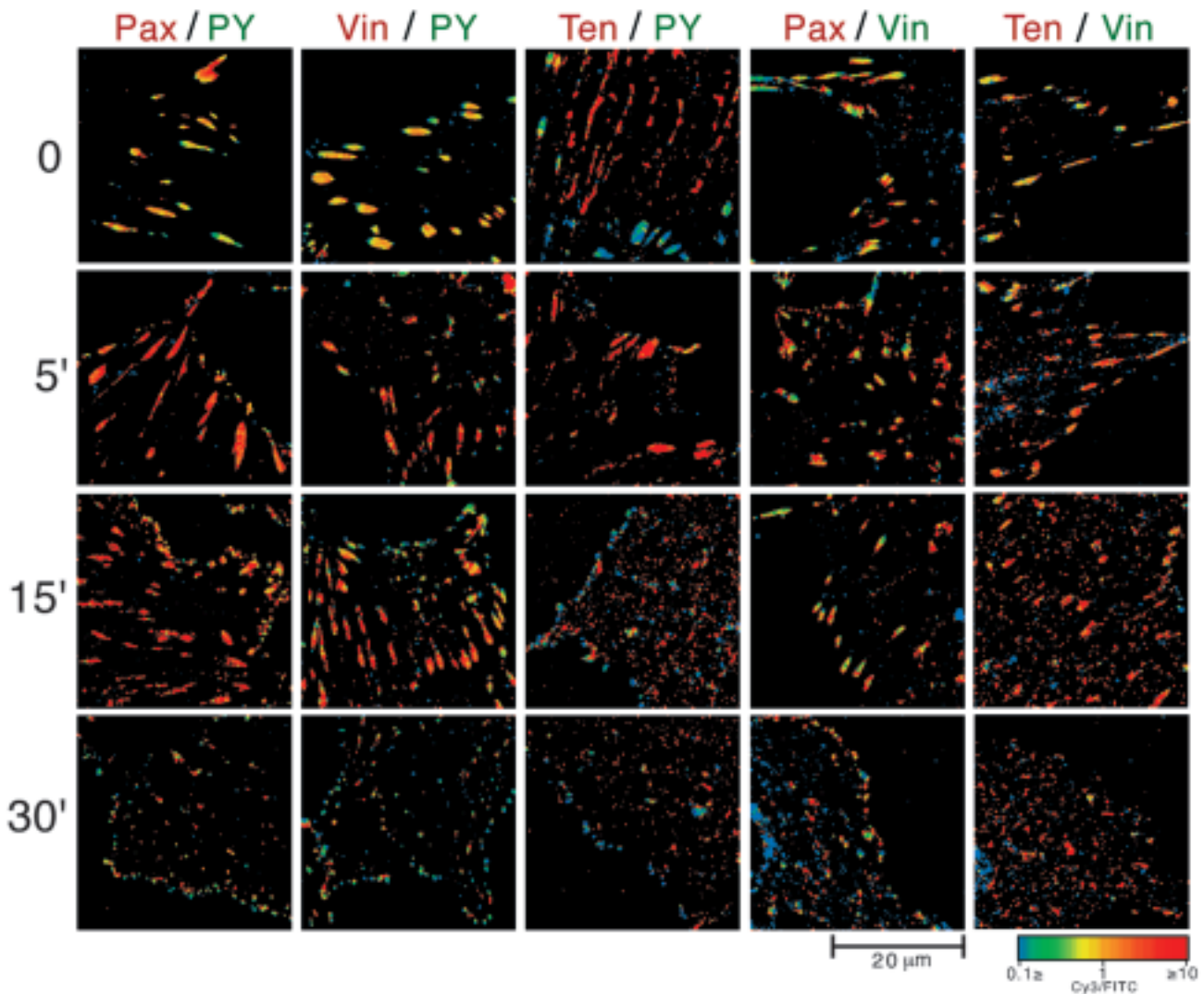


Fig. 11. FRI analysis following H-7-induced FC disassembly. REF52 cells, 48 hours after plating, were treated with 60 μM H-7 for 5, 15 or 30 minutes, fixed and double-labeled for phosphotyrosine (PY) and either paxillin, vinculin or tensin, and for vinculin with either paxillin or tensin. Untreated cells were used as controls. The protein names are colored red for Cy3 and green for FITC labeling. The ratio images, between the Cy3 and the FITC image, are presented in a spectrum scale representing the ratio value.

adhesion sites were reformed within 5 minutes after H-7 removal. The newly formed FC had apparently normal morphology, and their levels of paxillin, vinculin and phosphotyrosine were similar to those found in untreated cells (Fig. 12). Recovery of tensin in FC appeared to be somewhat slower.

DISCUSSION

The primary objective of the present study was to characterize the molecular and structural diversity, as well as the plasticity of cell-matrix adhesions. Studies for over two decades have revealed a multitude of so called 'FC proteins,' defined as such on the basis of their general distribution pattern. Yet, a standard and unequivocal definition of FC, their overall molecular compositions and potential diversity, have received relatively little attention. A major obstacle in approaching this issue in

the past has been the non-quantitative nature of most microscopic studies of FC structure. Thus, matrix adhesions are commonly viewed as a molecularly homogenous entity, containing a full repertoire of FC proteins (Burrige and Fath, 1989; Geiger et al., 1995; Jockusch et al., 1995).

In this study, we challenge this view and establish, with the help of digital microscopy, that matrix adhesions are highly diverse structures, both molecularly and morphologically, that can be subdivided into 3 main categories: (i) 'classical FC' which are arrowhead shaped, and contain high levels of phosphotyrosine, paxillin and vinculin, and relatively low levels of tensin, (ii) 'fibrillar adhesions' which are elongated (typical axial ratio >7) and contain relatively high levels of tensin and low phosphotyrosine, and (iii) 'mosaic FC' with the general appearance of classical FC, yet with a highly non-uniform internal molecular structure. We further show that treatment with the kinase inhibitor H-7, which blocks actomyosin-driven contractility, leads to a rapid loss of

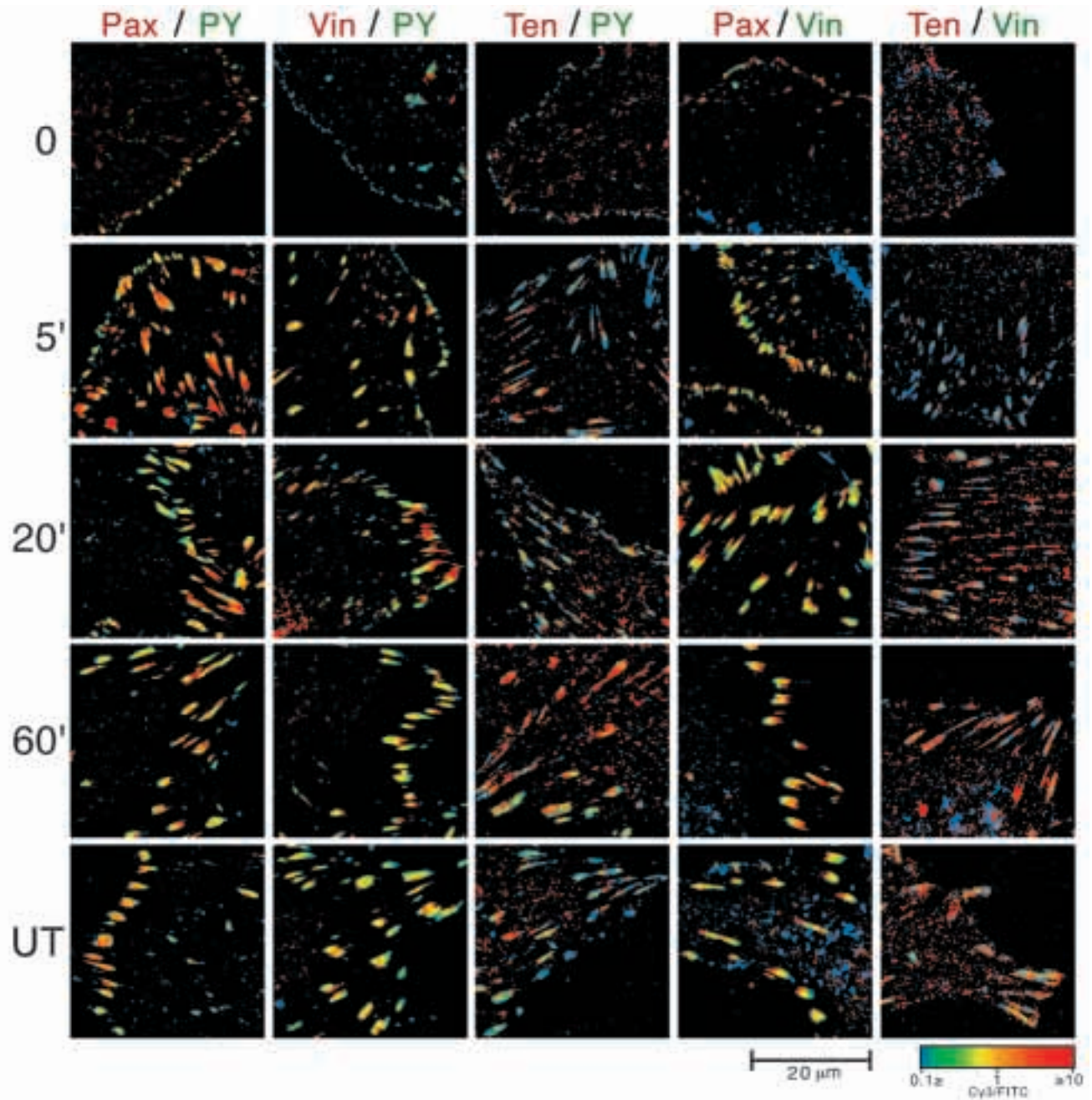


Fig. 12. FRI analysis of FC recovery following H-7 treatment. REF52 cells, 24 hours after plating, were treated with 60 μ M H-7 for 60 minutes. After nearly all FC had disassembled (time '0'), the H-7 was washed out, and the cells were further incubated in H-7-free medium for 5, 20 and 60 minutes, fixed and double-labeled as indicated, UT, untreated. The ratio images, between the Cy3 and the FITC image, are presented in a spectrum scale representing the ratio value.

phosphotyrosine from FC, followed by the disassembly of the structure. Re-assembly is swift (<5 minutes), suggesting that even large FC can be regenerated rapidly.

The key tool used here for studying matrix adhesion diversity was digital microscopy and multiple images processing, which enabled identification and molecular mapping of these sites. The novel elements in this analysis, described here for the first time, are the use of the *water* algorithm, the definition of criteria for an automatic recognition and segmentation of adhesion sites, and the

introduction of the ratio-imaging approach. Our initial attempts to use uniform (size and/or intensity) thresholds in order to eliminate background labeling failed to resolve individual adhesions, and large clusters of FC were often identified as a single structure. The *water* algorithm enabled identification of local 'valleys' which separate adjacent adhesion sites, resolving such clusters into the individual adhesions. The setting of critical area thresholds was selected empirically, so that fine substructures within individual adhesions would not lead to excessive segmentation. This precaution was especially

critical for fibrillar adhesions with granular labeling texture (such as the one shown in Fig. 2C). As indicated above, the segmentation process was carried out interactively, verifying that appropriate values of P_{\min}^f , A_{\min}^p and A_{\min}^m were selected, and allowing us to manually merge or separate adhesions. It is however noteworthy that such manual interventions were needed relatively rarely, and that the entire procedure enables a very broad and unbiased sampling of matrix adhesion sites, allowing for reliable statistical analyses.

A source of potential concern addressed in this study was the reliability of quantitation by immunofluorescence microscopy, namely, to what extent local fluorescence intensities accurately represent local concentrations of labeled proteins. This issue is relevant to interpretation of immunofluorescence data in general and is particularly critical in a quantitative study such as this report. To approach this issue, we compared the local intensities of fluorescence of GFP chimeras of vinculin, paxillin and tensin to the corresponding immunofluorescence images. Pixel-by-pixel comparisons of these images confirmed that the two were very closely correlated, indicating that, in these systems, levels of immunofluorescence intensity faithfully represent local protein concentrations and are not significantly affected by factors such as antigen exposure or epitope instability. It is nevertheless clear that these values provide information on the relative levels of the proteins in question and do not provide absolute protein concentrations.

A novel procedure described here is FRI of cytoskeletal and plaque proteins. As shown above, this approach was extremely useful in revealing the diversity in the molecular organization and sub-cellular distribution of matrix adhesions. It is, however, important to highlight here both the potential and limitation of this approach. The unique feature of FRI, which is not attainable by simple superposition, is that it is highly sensitive to local differences in relative fluorescence staining intensities of two proteins, irrespective of their absolute intensities, thereby providing valuable information for even faintly labeled structures. The calculations are based on 12-bit digital data, which are highly accurate even for faint structures. It should be emphasized that the calculated ratios are based on normalized fluorescence intensities (compensating for differences in overall labeling intensities with FITC-labeled and Cy3-labeled antibodies) and, as indicated above, they do not reflect the absolute concentrations of each of the molecules examined.

However, the data presented here on the differential distribution of various components of the submembrane plaque of matrix adhesions (vinculin, paxillin, tensin and phosphotyrosine) clearly document the diversity in the molecular organization of adhesion sites, as well as the presence of distinct molecular subdomains within these structures. We have distinguished here between 'classical' FC, 'fibrillar' adhesions, and 'mosaic' adhesions, based on the labeling for the four FC antigens listed above. Yet, it is entirely possible that systematic examination of additional plaque components (i.e. talin, focal adhesion kinase, VASP, α -actinin, actin, etc.; Geiger et al., 1995) will provide more comprehensive information on the detailed molecular organization of each type of adhesive structure. Such analysis is currently underway.

Another parameter examined in this study is the temporal

sequence of molecular interaction involved in the formation and modulation of matrix adhesions. Based on previous data, we have used the kinase inhibitor H-7 for the suppression of FC formation, and examined the disruption and reformation of adhesive structures upon its addition and removal. It has been previously shown that H-7 strongly suppresses actomyosin-driven contractility in cultured cells (Volberg et al., 1994) and that this effect leads to deterioration of stress fibers and FC (Bershadsky et al., 1996; Volberg et al., 1994; Tian et al., 1998). FRI analysis of cells at different time points after addition of H-7 indicated that the earliest detectable response to H-7 treatment was the loss of phosphotyrosine from FC. It is not clear yet whether this reduction in local phosphotyrosine levels is due to dephosphorylation in situ or to loss of phosphorylated proteins from the adhesion site. This effect was observed as early as 5 minutes after the addition of H-7, though at that stage proteins such as vinculin and paxillin were still retained in FC. Only following longer incubations a loss of these proteins from FC was observed along with deterioration of FC structure. We therefore propose that local tension applied by the actomyosin system may trigger local tyrosine phosphorylation, which, in turn, is important for the assembly of the submembrane plaque.

In a separate study (B. Z. Katz et al., unpublished), we have examined the integrin specificity of the various matrix adhesions in human foreskin fibroblasts. We found that classical FC contain mainly $\alpha_v\beta_3$, are devoid of fibronectin and are tyrosine-phosphorylated. The fibrillar adhesions, on the other hand, are $\alpha_5\beta_1$ - and fibronectin-rich and are poorly labeled for phosphotyrosine. It was further shown that local tyrosine phosphorylation heavily depends on matrix deformability, whereas tensin distribution closely correlates with that of $\alpha_5\beta_1$.

The results presented here on the molecular organization of matrix adhesion diversity, and the possibilities offered by the digital microscopic system described here, point to a remarkable molecular heterogeneity of these sites and offer a new classification of matrix adhesion subtypes. Further examination of matrix adhesion diversity after exposure of cells to a variety of additional experimental conditions such as differences in matrix molecules, growth factor stimulation, mechanical perturbations, microtubule reorganization and cell shape, may shed further light on the physiological assembly and reorganization of cell adhesion sites.

We thank Ken Nakata, Shingo Miyamoto and Kazue Matsumoto (NIDCR, NIH) for the human paxillin cDNA. We express our gratitude to Prof. Adi Shamir (Department of Applied Mathematics, the Weizmann Institute, Israel) for illuminating discussions. This study was supported by the Israel Science Foundation and the Minerva Foundation. BG holds the Erwin Neter Chair in Cell and Tumor Biology. ZK holds the Israel Pollak Chair of Biophysics

REFERENCES

- Abercrombie, M., Heaysman, J. E. and Pegrum, S. M. (1971). The locomotion of fibroblasts in culture. IV. Electron microscopy of the leading lamella. *Exp. Cell Res.* **67**, 359-367.
- Abercrombie, M. and Dunn, G. A. (1975). Adhesions of fibroblasts to substratum during contact inhibition observed by interference reflection microscopy. *Exp. Cell Res.* **92**, 57-62.
- Ayalon, O. and Geiger, B. (1997). Cyclic changes in the organization of cell

- adhesions and the associated cytoskeleton, induced by stimulation of tyrosine phosphorylation in bovine aortic endothelial cells. *J. Cell Sci.* **110**, 547-556.
- Bendory, R., Salomon, D. and Geiger, B.** (1989). Identification of two distinct functional domains on vinculin involved in its association with focal contacts. *J. Cell Biol.* **108**, 2383-2393.
- Bershadsky, A., Chausovsky, A., Becker, E., Lyubimova, A. and Geiger, B.** (1996). Involvement of microtubules in the control of adhesion-dependent signal transduction. *Curr Biol.* **6**, 1279-1289.
- Burridge, K. and Fath, K.** (1989). Focal contacts: transmembrane links between the extracellular matrix and the cytoskeleton. *BioEssays.* **10**, 104-108.
- Chen, H., Sedat, J. W. and Agard, D. A.** (1990). Manipulation, display, and analysis of three-dimensional biological images. In *Handbook of Biological Confocal Microscopy* (ed. J. B. Pawley), pp. 141-150. New York: Plenum Press.
- Chen, H., Swedlow, J. R., Grote, M., Sedat, J. W. and Agard, D. A.** (1995). Collection, processing, and display of digital three-dimensional images of biological specimens. In *Handbook of Biological Confocal Microscopy* (ed. J. B. Pawley), pp. 197-210. New York: Plenum Press.
- Clark, E. A. and Brugge, J. S.** (1995). Integrins and signal transduction pathways: the road taken. *Science* **268**, 233-239.
- Cormack, B. K., Valdivia, R. H. and Falkow, S.** (1996). FACS-optimized mutants of the green fluorescent protein (GFP). *Gene* **173**, 33-38.
- Geiger, B.** (1979). A 130K protein from chicken gizzard: its localization at the termini of microfilament bundles in cultured chicken cells. *Cell* **18**, 193-205.
- Geiger, B., Yehuda-Levenberg, S. and Bershadsky, A. D.** (1995). Molecular interactions in the submembrane plaque of cell-cell and cell-matrix adhesions. *Acta Anat. (Basel)*. **154**, 46-62.
- Gilmore, A. P. and Burridge, K.** (1996). Molecular mechanisms for focal adhesion assembly through regulation of protein-protein interactions. *Structure* **4**, 647-651.
- Heath, J. P. and Dunn, G. A.** (1978). Cell to substratum contacts of chick fibroblasts and their relation to the microfilament system. A correlated interference-reflexion and high-voltage electron-microscope study. *J. Cell Sci.* **29**, 197-212.
- Hynes, R. O.** (1987). Integrins: a family of cell surface receptors. *Cell* **48**, 549-554.
- Hynes, R. O.** (1992). Integrins: versatility, modulation, and signaling in cell adhesion. *Cell* **69**, 11-25.
- Izzard, C. S. and Lochner, L. R.** (1976). Cell-to-substrate contacts in living fibroblasts: an interference reflexion study with an evaluation of the technique. *J. Cell Sci.* **21**, 129-159.
- Jockusch, B. M., Bubeck, P., Giehl, K., Kroemker, M., Moschner, J., Rothkegel, M., Rudiger, M., Schluter, K., Stanke, G. and Winkler, J.** (1995). The molecular architecture of focal adhesions. *Annu. Rev. Cell. Dev. Biol.* **11**, 379-416.
- Kam, Z., Jones, M. O., Chen, H., Agard, D. A. and Sedat, J. W.** (1993). Design and construction of an optimal illumination system for quantitative wide-field multi-dimensional microscopy. *Bioimaging* **1**, 71-81.
- Kam, Z., Volberg, T. and Geiger, B.** (1995). Mapping of adherens junction components using microscopic resonance energy transfer imaging. *J. Cell Sci.* **108**, 1051-1062.
- Kam, Z., Agard, D. A. and Sedat, J. W.** (1997). Three-dimensional microscopy in thick biological samples: a fresh approach for adjusting focus and correcting spherical aberration. *Bioimaging* **5**, 40-49.
- Kioka, N., Sakata, S., Kawauchi, T., Amachi, T., Akiyama, S. K., Okazaki, K., Yaen, C., Yamada, K. M. and Aota, S. I.** (1999). Vinexin: a novel vinculin-binding protein with multiple SH3 domains enhances actin cytoskeletal organization. *J. Cell Biol.* **144**, 56-69.
- Miyamoto, S., Teramoto, H., Coso, O. A., Gutkind, J. S., Burbelo, P. D., Akiyama, S. K. and Yamada, K. M.** (1995). Integrin function: molecular hierarchies of cytoskeletal and signaling molecules. *J. Cell Biol.* **131**, 791-805.
- Price, G. L., Jones, P., Davison, M. D., Patel, B., Bendori, R., Geiger, B. and Critchley, D. R.** (1989). Primary sequence and domain structure of chicken vinculin. *Biochem. J.* **259**, 453-461.
- Sambrook, J., Fritsch E. F. and Maniatis T. M.** (1989). *Molecular Cloning: A Laboratory Manual*. Cold Spring Harbor, NY: Cold Spring Harbor Laboratory Press.
- Schwartz, M. A., Schaller, M. D. and Ginsberg, M. H.** (1995). Integrins: emerging paradigms of signal transduction. *Annu. Rev. Cell. Dev. Biol.* **11**, 549-599.
- Soferman, Z.** (1989). *Computerized Optical Microscopy*. Doctoral thesis. Department of Applied Mathematics and Computer Science. Weizmann Institute of Science, Rehovot, Israel.
- Tian, B., Millar, C., Kaufman, P. L., Bershadsky, A., Becker, E. and Geiger, B.** (1998). Effects of H-7 on the iris and ciliary muscle in monkeys. *Arch. Ophthalmol.* **116**, 1070-1077.
- Turner, C. E., Glenney, J. R., Jr. and Burridge, K.** (1990). Paxillin: a new vinculin-binding protein present in focal adhesions. *J. Cell Biol.* **111**, 1059-1068.
- Usson, Y., Guignandon, A., Laroche, N., Marie-Helene, L. P. and Vico, L.** (1997). Quantitation of cell-matrix adhesion using confocal image analysis of focal contact associated proteins and interference reflection microscopy. *Cytometry* **28**, 298-304.
- Volberg, T., Zick, Y., Dror, R., Sabanay, I., Gilon, C., Levitzki, A. and Geiger, B.** (1992). The effect of tyrosine-specific protein phosphorylation on the assembly of adherens-type junctions. *EMBO J.* **11**, 1733-1742.
- Volberg, T., Geiger, B., Citi, S. and Bershadsky, A. D.** (1994). Effect of protein kinase inhibitor H-7 on the contractility, integrity, and membrane anchorage of the microfilament system. *Cell Motil Cytoskel.* **29**, 321-338.
- Yamada, K. M.** (1997). Integrin signaling. *Matrix Biol.* **16**, 137-141.
- Yamada, K. M. and Geiger, B.** (1997). Molecular interactions in cell adhesion complexes. *Curr. Opin. Cell Biol.* **9**, 76-85.
- Yamada, K. M. and Miyamoto, S.** (1995). Integrin transmembrane signaling and cytoskeletal control. *Curr. Opin. Cell Biol.* **7**, 681-689.